6

Remote Sensing Techniques for Forest Fire Disaster Management: The FireHub Operational Platform

Charalampos Kontoes, Ioannis Papoutsis, Themistocles Herekakis, Emmanuela Ieronymidi, and Iphigenia Keramitsoglou

CONTENTS

Introduction

Wildfires have always been present in Mediterranean ecosystems and thus constitute a major ecological and socioeconomic concern. During the last decades, both the number and average size of large fires have experienced an increasing trend, causing extensive economic and ecological losses and often human casualties (Dimitrakopoulos and Mitsopoulos 2005). Increased wildland fire activity over the last 30 years has had profound effects on the budgets and operational priorities of the forest services, civil protection agencies, fire brigades, and local entities with wildland fire management responsibilities (Giannakopoulos et al. 2009; Dimitrakopoulos et al. 2011; Koutsias et al. 2013). Significant alterations in the fire regime have occurred in recent decades, primarily as a result of socioeconomic changes, increasing dramatically the catastrophic impact of wildfires. Despite the recent advances in firefighting tactics and means and the increased amount of resources allocated for fire suppression, the efficiency of the adopted strategy has been decreasing over the last four decades, with both number of fires and burnt area increasing (Bassi et al. 2008).

In this context, the development of appropriate fire suppression strategies for wildfires is challenging. A careful reconsideration of the current wildfire management strategy is necessary in order to reduce the devastating impacts of wildfires on an ecosystem's ecological integrity, society, and economic activity in the future. Fire managers are required to consider and balance threats to multiple socioeconomic and environmental resources and need to identify, in real time, the probability that a wildfire will affect valuable resources and disrupt activities, as well as to estimate the level of damage in ecosystems. The development of more effective wildfire management strategies is a real necessity and requires the availability of accurate and spatially explicit data in order to support evidence-based decision-making.

Earth observation (EO) technology can provide such evidence, through the systematic and standardized processing of satellite imagery. In this context, a large number of EO images of different spectral and spatial resolutions are exploited by the National Observatory of Athens (NOA) through BEYOND (Building a Centre of Excellence for EO-Based Monitoring of Natural Disasters; www.beyond-eocenter.eu), in order to derive thematic products that cover a wide spectrum of wildfire management applications. These products address the requirements of crises occurring before, during, and after fires and follow the Copernicus (GMES) Emergency Response and Emergency Support standards (http://emergency.copernicus.eu/). The NOA has developed a portfolio of similar products, including early fire detection, fire monitoring, and rapid fire mapping, as well as weekly, seasonal, and diachronic burn scar mapping (BSM) and land use/land cover damage assessments over the affected areas.

The concept is to rely on the effective integration of satellite imagery with auxiliary geospatial information and meteorological data, based on statistical and rule-based methods. Input satellite data are comprised of multispatial, multitemporal, and multispectral remote sensing data from EUMETSAT, NASA, NOAA, and European Space Agency missions, and the incorporated processing chains are scalable *via* the exploitation of array database and semantic Web technologies (Koubarakis et al. 2012).

The FireHub real-time fire monitoring service is operated on a routine basis by the BEYOND Center of Excellence, which provides continuous information on active fires detected from EO satellites. The system ingests raw satellite images of coarse spatial resolution from the SEVIRI instrument on board the Meteosat Second Generation (MSG) series of satellites, providing data every 5 minutes. In addition, medium resolution images captured by the moderate-resolution imaging spectroradiometer (MODIS) onboard the Earth Observing System (EOS) Aqua and Terra satellites, the Visible Infrared Imaging Radiometer Suite (VIIRS) onboard the Suomi National Polar-Orbiting Partnership (NPP) satellite, the advanced very high resolution radiometer (AVHRR) onboard the EUMETSAT MetOp, and NOAA Polar Operational series of satellites, with a revisiting capacity of a few hours a day, are automatically ingested into the system by the time of acquisition. Finally, the FireHub system design foresees that in the immediate future, high-resolution Sentinel-2 data will become available in real time through the Hellenic National Sentinel Data Mirror Site (http://sentinels.space.noa.gr), which is part of the ESA's Collaborative Ground Segment in Southeastern Europe. The workflow integrates a number of geospatial layers and *in situ* data representative of the area's fuel model, the topography, and the dynamic meteorological forecasts relevant to wind speed and wind direction. The system provides on a 5-minute basis, and with a time interval of less than 6 seconds after the satellite image acquisition, a fine-grained classification of fire occurrence in subpixels of 500×500 m wide, thus improving the initial MSG/SEVIRI raw observation by about 50 times.

In addition to early fire detection and monitoring, the identification and recording of the burnt areas is routinely achieved through the implementation of a remote sensing method explicitly developed at the NOA for BSM (the BSM-NOA method). The applied BSM-NOA method (Kontoes et al. 2009) was developed and deployed in the framework of the Copernicus (GMES) European flagship program. It aims to contribute to a standardized and homogeneous mapping of burnt areas and related vegetation damage in the European Union member states. The system ensures timely production of burnt area maps, from 1 day (for specific fires that need rush-mode mapping) to a few days (for emergency support), or up to 2 months after the end of the fire season to cover the national scale demands with high thematic and spatial accuracy. This activity supports the reporting and planning needs of the operational users nationwide.

Today, after several development phases, it is delivered through the BEYOND Center of Excellence to the wide institutional user community—ministries of environment, forestry services, and civil protection authorities—and it has been approved as a robust and accurate method. The method has a high spatial precision (0.5–1 ha), at desirable mapping scales ranging from 1:10,000 to 1:50,000. Specifically for Greece, the service is provided *via* a Web GIS application. It serves a yearly updated geodatabase that contains the results of the diachronic burnt area mapping over the country since 1984. Its production was based on analysis of the full USGS archive of Landsat Thematic Mapper (TM) images, since the first satellite image was ever recorded over Greece.

This chapter describes the theoretical background, architecture, and performance characteristics of these two fully automated Web GIS–based systems (fire monitoring and fire mapping) that are designed to assist land managers in wildfire suppression planning and in postfire damage assessment. They consist of the two basic modules of the so-called FireHub

Platform (http://ocean.space.noa.gr/FireHub), which was awarded first prize for Best Challenge Service in the Copernicus Masters Awards Competition 2014.

Theoretical Background

Real-Time Fire Monitoring

Real-time fire activity has shown great potential to be detected from polar orbiters (Giglio et al. 2003) and geostationary satellites (Calle et al. 2006). Polar orbiters are capable of providing data at moderate to high resolution, whereas data from geostationary satellites have proven to be useful for the detection of fire activity at continental and global scales and offer broad direct broadcast capabilities. Polar orbiters provide only four observations per day of approximately 1 km spatial resolution at nadir. High variance of the detectable hotspots and temporal sampling issues related to the diurnal fire cycle have been reported. In contrast, geostationary satellites offer great advantages in filling in the gaps in spatial coverage worldwide at high temporal rates (5–15 minutes), although with a much coarser spatial resolution (approximately 4–5 km) (Prins and Menzel 1996).

In the literature we found EO-based fire-detection studies that were mainly based on the use of radiometers, such as the AVHRR—a space-borne sensor onboard the NOAA family of polar-orbiting platforms that measures the reflectance of the Earth in five relatively wide spectral bands (Chuvieco and Martin 1994). Another well-documented and tested sensor, widely used in active fire detection, is MODIS, which is equipped on the EOS and operates on both the Terra and Aqua spacecrafts (Kaufman et al. 1998). Several operational systems have been developed worldwide using the two abovementioned sensors for active fire-detection purposes. The Global Fire Information Management System delivers MODIS hotspot/fire location information to natural resource managers and other stakeholders around the world (Justice et al. 2002). In Europe, the European Forest Fire Information System (EFFIS) maps active hotspots using MODIS and provides a synoptic view of current fires in Europe as a means to assist the subsequent mapping of burnt area perimeters. Information on active fires is nominally updated on a daily basis and, when needed, made available in EFFIS within 2–3 hours of the MODIS image acquisition (San-Miguel-Ayanz et al. 2005).

Regional operational active fire-detection systems also exist. The German Remote Sensing Data Center of the German Aerospace Center offers an operational service on fire detection from space. Based on data obtained from the experimental satellite BIRD and from MODIS, wildfires are detected and mapped (Brieb et al. 1996). In Canada, the Canadian Fire Monitoring, Mapping, and Modelling System uses infrared imagery from NOAA/AVHRR for the daily monitoring of active fires and smoke across the country. This information is further used to derive estimations of fire impact and fuel consumption at a national scale (Li et al. 2000). In Australia, the FireWatch Map Service provides emergency services personnel with an online mapping application to help in fire management over the continent. The data sets include fire hotspots from MODIS and NOAA imagery (Steber et al. 2012). The Remote Sensing Laboratory of the University of Valladolid in Spain provides public operational information on fires detected from geostationary MSG/SEVIRI in some countries of Western Europe and North Africa, with 15-minute information updates and disseminates the results over the Internet (Pennypacker et al. 2013).

Despite its coarse spatial resolution, several studies have demonstrated the capabilities of the SEVIRI instrument for the detection of fires with a size much smaller than the resolution cell. Two of SEVIRI's spectral bands are operative in the shortwave infrared (SWIR) (3.9 μm) and thermal infrared (10.8 μm) wavelengths, and they are sensitive to fire and to Earth's surface radiative temperature. Laneve et al. (2006) reported that MSG/SEVIRI can be used to detect fires up to a relatively small size (0.1 ha) with a synoptic view of their distribution on a large scale, thus allowing for a more efficient and operational fire-suppression component. In the same context, Van den Bergh and Frost (2005) employed multitemporal approaches to detect fires based on the high update rate of MSG/SEVIRI, while Umamaheshwaran et al. (2007) investigated the potential application of an image mining method for monitoring and analyzing fire behavior in high-resolution scale in order to improve the information extracted from MSG/SEVIRI.

The potential of MSG/SEVIRI was in fact promptly explored, namely within the scope of characterizing the spatiotemporal distribution of wildfire activity on the African continent (Amraoui et al. 2010), as well as estimating the amounts of released fire intensity and fuel consumption (Roberts and Wooster 2008). In Europe, MSG/SEVIRI images were incorporated in processing workflow in order to develop a real-time detection system for Greek territory (Sifakis et al. 2011). MSG imagery has shown good results when used for generating fire risk maps based on fire weather indexes for the Mediterranean basin (Amraoui et al. 2013).

Burn Scar Mapping

Several studies have shown that remotely sensed imagery acquired in various spatial, spectral, and temporal resolutions is an effective means to delineate the burnt areas and to determine the species affected and the degree of damage caused (Sifakis et al. 2004; Quintano et al. 2006). Burn scars can be clearly identified on a variety of satellite image acquisitions like those from NOAA/AVHRR, Landsat TM and Enhanced TM+ (ETM+), MODIS, the medium-resolution imaging spectrometer Satellite Pour l'Observation de la Terre, and Indian Remote Sensing satellites (e.g., Fung and Jim 1998; Koutsias 2000; Koutsias and Karteris 2000; Rogan and Yool 2001; Chuvieco et al. 2002;

Fraser and Li 2002; Pu and Gong 2004; Gong et al. 2006). In practice, satellite-based BSM takes advantage of the distinctive spectral response of burnt vegetation. While healthy, living vegetation reflects near-infrared (NIR) radiation and absorbs red light in the visible (VIS) part of the spectrum, burnt areas reflect comparatively more radiation in the VIS and SWIR parts of the spectrum and absorb radiation in the NIR. This is attributed to the destruction of the plant and leaf structure (Rogan and Yool 2001). Subsequently, elimination of healthy green vegetation and the inevitable presence of charcoal or bare soil in the fire zone result in a change of radiation recorded by satellite sensors in the relevant spectral bands. These spectral discrepancies between pre- and postfire image acquisitions allow for a clear identification of the burnt area boundaries.

For automatic fire mapping, different methods are employed. The choice is largely dependent on the types of satellite data (spectral and spatial resolutions), the area landscape characteristics (mixed land cover classes, fragmented landscape, and mixed forests with agriculture), and the size of the study area (region, country, and continent). These methods may include fixed thresholding algorithms, adaptive thresholding contextual algorithms (Li et al. 2001), or an integration of the two (Gong et al. 2006) applied to image spectral bands and/or computed indices derived from uni- or multitemporal image acquisitions. Apart from data thresholding techniques, there exist diverse methods, employing logistic regression, exploiting image-derived indices (e.g., vegetation indices) coupled with geographic data (Koutsias 2000), approaches using linear and/or nonlinear spectral mixture analysis techniques (Sa et al. 2003; Ustin 2004), rule-based tree classification (Simard et al. 2000), and neural network (Pu and Gong 2004) methods.

Extraction of burnt land information from remotely sensed data can be performed by using either uni- or multitemporal image acquisitions. Three different approaches have been reported including the following: (1) application of multiple tests on spectral values and indices derived from unitemporal data; (2) multitemporal change analysis of spectral and biophysical indices; and (3) image segmentation and classification techniques using uni- or multitemporal data (Arino et al. 1999). In the first approach, the identification of burnt areas is performed by analyzing the spectral differences of image bands and image-derived indices (e.g., Normalized Burn Ratio Index; Key and Benson 2003) using a single postfire image (Pereira 1999). In certain projects, this approach is preferred to a multitemporal one, as it makes the analysis straightforward. In the second approach, the temporal changes of spectral and/or biophysical parameters due to fires are detected using two images, pre- and postfire (Martin and Chuvieco 1995; Miller and Yool 2002; Fisher et al. 2003). Analyzing the postfire decrease of vegetation vigor (e.g., multitemporal change analysis of vegetation indices), the changes depicted in multitemporal principal component analysis (PCA) vectors (Fisher et al. 2003), or even the changes of brightness, greenness, and wetness components introduced by the so-called tasseled cap Kauth–Thomas transform (Collins and Woodcock 1996), the burnt areas can be identified and mapped more effectively than using a single image. In addition, this approach minimizes the spectral confusion of burnt areas with other land cover types such as permanent crops, open agricultural fields, shadows, and urban and water surfaces. The third method involves conventional image classification and postclassification of uni- or multitemporal satellite data and image-derived indices.

NOA's FireHub Real-Time Forest Fire Detection and Monitoring Service

The System Architecture

The real-time fire monitoring platform delivers an integrated fully automatic processing chain. This module is part of the FireHub service of the BEYOND Center of Excellence. It is divided into dedicated subsystems that offer stakeholders online access to robust, accurate, and fully operational Web-accessible products to assist in fire management and decision-making. The system is enhanced *via* the integration of innovative information technologies for the effective storage and management of the large amount of EO and GIS data, the postprocessing refinement of fire products using semantics (Kyzirakos et al. 2014), and the timely creation of fire extent and damage assessment thematic maps (Figures 6.1 and 6.3).

The architecture of this fully automated forest fire–monitoring application consists of the following parts:

1. Satellite Ground Segment facilities (Block 1 of Figure 6.1) comprise the following:
   a. The high-throughput *MSG/SEVIRI ground-based receiving antenna* (DVB-S2), which collects all spectral bands from any available Meteosat satellite every 5 or 15 minutes, depending on the satellite platform.
   b. The *X-/L-band receiving antenna*, which provides real-time acquisitions from NASA, NOAA, and third-party satellite missions such as the Earth Observing System (EOS), NPP, JPSS, NOAA/AVHRR, MetOp, and FengYun systems.
   c. The *ESA's Sentinel Collaborative Ground Segment (mirror site) infrastructure*: The so-called mirror site of the NOA provides real-time acquisitions of the ESA Sentinel 1, 2, and future 3 and 5P missions, covering the geographic area of Southeastern Europe, the Balkans, North Africa, and the Middle East. The mirror site has been designed to connect with the backbone of the GEANT network (http://www.geant.net/) for fast access to the image data from ESA's core ground segment.

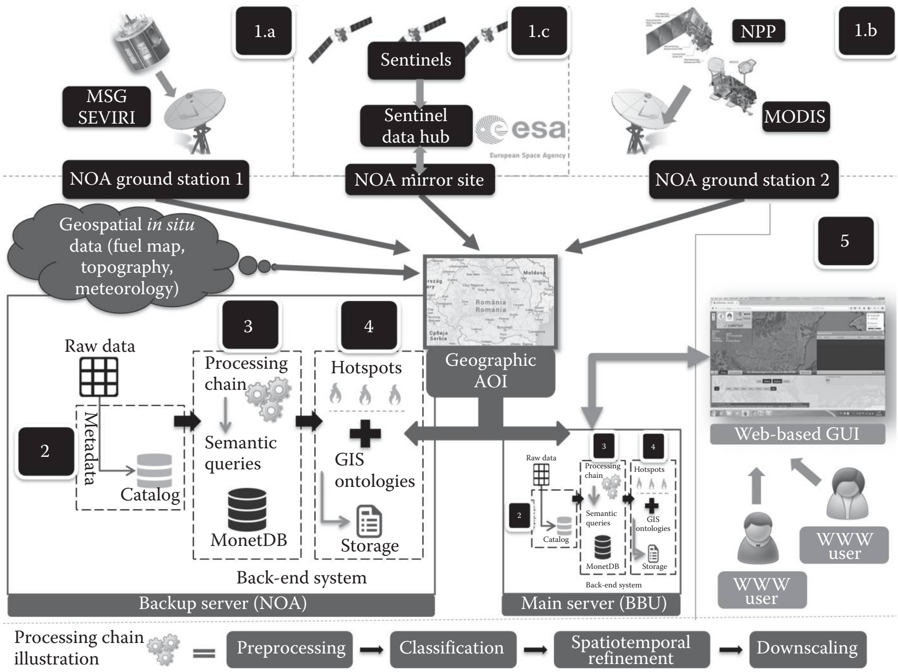

FIGURE 6.1
Architecture of the real-time forest fire detection and monitoring module of the FireHub tool.

2. The raw image data sets that are decoded and temporarily stored in the data vault. This system is responsible for the ingestion policy and enables the efficient access to large archives of image data and metadata in a fully transparent way, regardless of their format, size, and location (Block 2 of Figure 6.1).
3. The back end of the system (Figure 6.3). The back end relies on array image processing solutions such as MonetDB (https://www.monetdb.org/) for two tasks: (1) the implementation of the fire hotspot detection processing chain (using the SciQL scientific query language, https://en.wikipedia.org/wiki/MonetDB#SciQL) and (2) the evaluation of semantic queries for improving the accuracy of the products and rapidly generating thematic maps (using the semantic spatiotemporal Resource Description Framework [http://www.w3.org/RDF] store Strabon [http://www.strabon.di.uoa.gr/]) (Block 3 of Figure 6.1).
4. A geospatial ontology that links the generated hotspot products (probable active fire pixels) with stationary GIS data (Corine Land Cover, Coastline, Administrative Geography) and open geospatial data available on the Web (e.g., LinkedGeoData—http://linkedgeodata.org/,

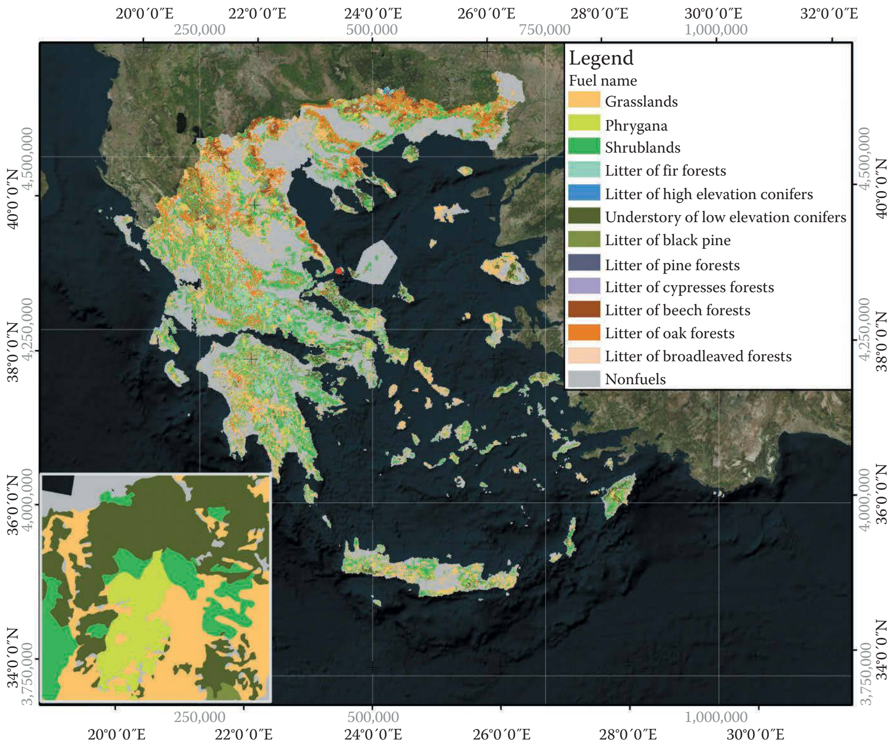

FIGURE 6.2
Fuel map of Greece, generated from the update and fusion of detailed governmental land use databases with the Corine Land Cover data.

GeoNames—http://www.geonames.org/). This ontology is expressed in Web Ontology Language (Block 4 of Figure 6.1 and Block 2 of Figure 6.3).

5. The spatial resolution refinement process, which employs a complex model for the improvement of the spatial accuracy of the satellite-based observations by approximately 50 times, thus downscaling the hotspot spatial resolution from cells of 3.5 × 3.5 km to cells of 500 × 500 m. The algorithms behind this process are currently being evaluated for awarding a patent (Block 3 of Figure 6.3).
6. The submodule for the ingestion of meteorological model forecasts. It consists of a 52-hour wind speed and wind direction prediction, with a 4-km spatial resolution at a fixed grid and a temporal resolution of 1 hour (Block 4 of Figure 6.3).
7. The sun module that feeds large-scale and high-specificity fuel information, as depicted in Figure 6.2. This map was derived through the

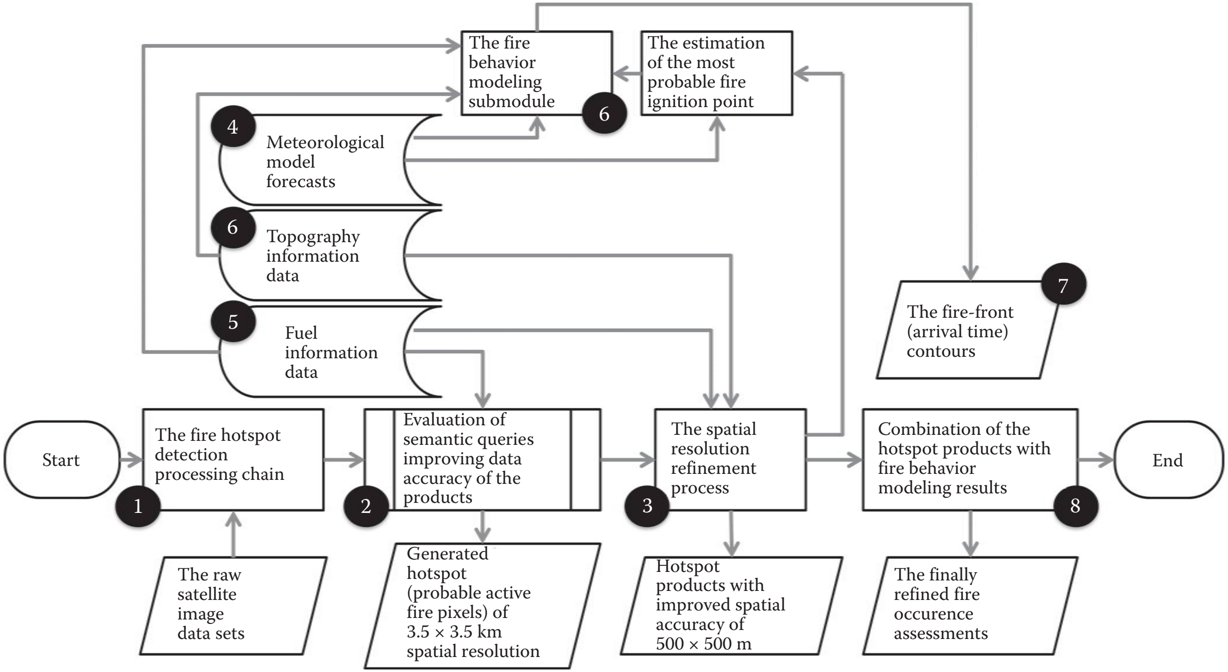

FIGURE 6.3
The main algorithmic blocks of FireHub's fire monitoring process.

fusion of the major vegetation classes represented in existing land use databases with the Corine Land Cover 2000 database. The fuel-type generation was based on a reclassification procedure and conversion of the vegetation types into custom fuel models representative for Greek ecosystems (Block 5 of Figure 6.3).

8. The module that processes the 30 × 30 m ASTER Global Digital Elevation Map tiles for deriving the slope and aspect information parameters in each 500 × 500 m cell (Block 5 of Figure 6.3).
9. The fire behavior modelling submodule, which automatically invokes in specific time frames the FlamMap (Finney 2006) fire model (Block 6 of Figure 6.3); the output of the model (Block 7 of Figure 6.3) is combined with the real-time satellite observations for deriving refined fire occurrence assessments (Block 8 of Figure 6.3).
10. The front-end interface, for controlling the back-end functionality with user-friendly tools, controlling the appearance of the information layers in the monitor, and disseminating the products to the end-user community through the Web (Block 5 of Figure 6.1).

The graphical user interface provides several functionalities for serving the hotspot and the smoke dispersion forecasts *via* the Web GIS interface. These are as follows: (1) the systematic provision every 5 minutes of the fire extent; (2) the retrieval and display of past fire events; and (3) the systematic provision on an hourly basis of smoke plume dispersion in 2D and 3D. Active fires are displayed in (1) refined mode (500 × 500 m wide cells) and (2) raw mode (~3.5 × 3.5 km wide cells). Three background map layers can be selected as background maps: (1) the LSO/VLSO Orthophotos of Ktimatologio S.A. (http://www.ktimatologio.gr), which is a detailed raster basemap with a spatial resolution of 1 m; (2) Google Earth tiles; and (3) the CORINE Land Cover (2000).

Methodology and System Operations

The following operations are invoked on a routine basis every 5 minutes, as soon as a new MSG/SEVIRI satellite image is ingested into the system from the receiving station. It should be acknowledged that the different processing steps, the description of which follows, have been developed and validated in the frameworks of the TELEIOS ICT (http://www.earthobservatory.eu/) and BEYOND EC projects (http://beyond-eocenter.eu/). For more detailed information, a rich compilation of related publications stemming from research work in the framework of these projects is available to the reader through the projects' websites.

Figure 6.3 shows the general methodology used for the incorporation of the minimum travel time (MTT) algorithm in NOA's FireHub real-time fire detection and monitoring system.

First, each pixel of a new satellite acquisition is classified either as *fire*, *potential fire*, or *nonfire*. However, the inherent coarse resolution of the MSG/SEVIRI instrument results in false alarms and omission errors, which reflect on the product's accuracy. The accuracy of the algorithm is enhanced by combining the first classification outcome with external information from linked geospatial data.

For example, a typical shortcoming of the original classification is false alarms at locations with inconsistent land use, such as urban or agricultural areas. This problem is overcome by using a data set that describes the Greek ecosystems in terms of land use/land cover classes and removing those early detected hotspots in nonvegetated areas. The hotspot product, generated every 5 minutes, is subsequently passed through a series of refinement steps to increase its accuracy and robustness by respecting several spatiotemporal fire behavior rules. Indicatively, the temporal persistence of a fire pixel over a period of, say, half an hour increases the confidence level (CL) that it is correctly classified as fire. Therefore, these operations primarily focus on updating the CL of each hotspot pixel and thus moving from the three-flag approach (fire, potential fire, and nonfire) to a real CL value. In addition, the refined hotspot is annotated with the region name it belongs to as attribute information.

Finally, the requirement to generate added-value thematic maps is addressed at this processing level. The Linked Open Data Cloud supplies an abundance of data sets, ranging from fine-grained geometric objects like fire stations to coarser ones like countries. Therefore, instead of manually combining heterogeneous data, the user can design a semantic query to integrate and overlay information layers, generate maps, and export data in well-established formats (Kyzirakos et al. 2012). Although this service was designed for Greece, it can be applied to any geographic area due to the open technologies adopted.

The next step is particularly important because it improves the spatial resolution of fire detection. At this processing phase, each MSG/SEVIRI pixel corresponding to a fire or potential fire event is divided into a 7×7 grid, that is, to subpixels of 500×500 m. For each of these 500-m wide cells, a new CL for fire occurrence is calculated with the use of specific fire hazard weight factors. Such factors take into account the probability of fire occurrence and ease of fire propagation, for example, topography and vegetation characteristics. The new CL is the product of the raw CL (CL_{raw}), with the weight factors derived from the fuel type (W_{FT}), elevation (W_E), slope (W_S), aspect (W_A), and fuel cover (W_{FD}) weights. The normalization of the weight factors and therefore their contribution to the calculation of follows the suggestions of Kontoes et al. (2013a).

$$CL = CL_{raw} \times W_E \times W_S \times W_A \times W_{FT} \times W_{FD} \quad (6.1)$$

Moreover, the MTT algorithm (Finey 2002) is used for modeling the fire propagation in each event, as embedded in the FlamMap fire behavior

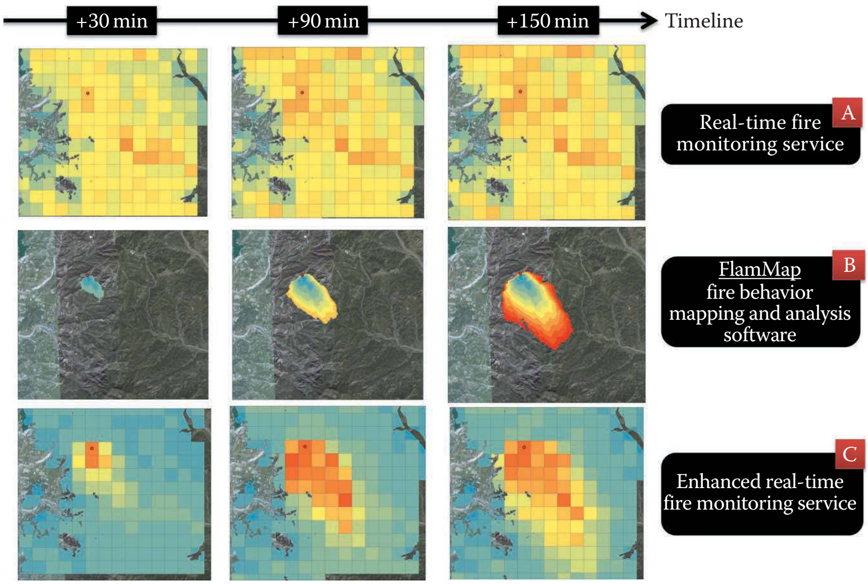

FIGURE 6.4
A typical fire evolution example at the different processing levels of FireHub.

software. FlamMap calculates the fire size and shape from an ignition point. The output of the model is compared in terms of its spatial distribution and temporal evolution to the fire event's pixel observations with the MSG/SEVIRI image. From this point on, a complex modeling scheme is implemented that fuses the information from the fire pixel classification CL and the fire propagation model output to derive the refined fire occurrence evidences in each 500 × 500 m subpixel.

A typical example of a fire evolution event in 2013, on the island of Rhodes, Greece, is presented in Figure 6.4. The products generated at the various processing levels of the FireHub system are shown. The first row in Figure 6.4 shows the downscaled hotspots after the first satellite imagery classification (CL), the second row corresponds to the integration of the FlamMap dispersion model results, and the last row is the final result delivered to the end-user community, which is the outcome of the combination of the satellite observation after integrating the simulated fire dispersion forecast product.

NOA's FireHub BSM and Damage Assessment Service

This is a fully automatic single or multidate processing chain that takes as input multispectral satellite images of any spatial resolution and produces precise burnt area polygons and wildland area damage assessments over

Greek territory (Kontoes et al. 2013a). The service follows the Copernicus (GMES) accuracy and validation standards and it has been successfully evaluated over different territories in Southeastern Europe. As such, it has been qualified and is transferable to any place over Europe at the regional, national, and continental levels. The burn scar mapping (BSM-NOA) service was initially developed in the framework of the ESA GMES Service Element program called *Risk-EOS*, the so-called BSM-NOA service (Kontoes et al. 2009), and has been fine tuned to become a fully operational processing chain.

The BSM-NOA service is activated on a user-demand basis, and the burnt area products are delivered to end users either in rush mode for emergency response purposes or in nonrush mode within a few days after the suppression of the fire event for emergency support purposes, and also immediately after the end of the fire season to meet recovery needs for the entire region/country. Depending on the input satellite data, the service provides BSMs at high spatial resolution (20–30 m pixel size, minimum detected fire size of 1 ha) and very high spatial resolution (2–8 m pixel size, spatial accuracy of 4–10 m, detected fire size of 0.5 ha), as well as damage assessments at the landscape level.

Based on the BSM-NOA core processing algorithm, a multitemporal analysis is feasible to estimate the annual burnt areas spanning several years. Such an analysis provides a diachronic mapping product that can be exploited for further statistical analyses, fire behavior cyclic patterns, climate change studies, and so on. For the production of the diachronic BSM of Greece, the entire USGS Landsat TM imagery archive over Greece since 1984 was used—that is, the first year when Greece was captured by the Landsat TM sensor. Figure 6.5 depicts the main steps of the BSM-NOA production chain.

The processing chain is divided into three stages, each one containing a series of modules:

1. The preprocessing stage:
   a. Identifying appropriate satellite data (spatial/spectral resolution, coverage, and acquisition dates), downloading, and archiving (Block 1a of Figure 6.5).
   b. *Radiometric normalization, registration, and georeferencing:* A fully automatic procedure wherein the input raw satellite images are calibrated, pixel values are converted from digital counts to radiometric values, and automatic image orthorectification is performed (Gao et al. 2009) (Block 1b of Figure 6.5).
   c. *Cloud/water masking:* The generation of a mask to exclude from subsequent processing pixels "contaminated" by clouds, as well as pixels representing water areas. This is done using NASA's LEDAPS algorithm (http://ledaps.nascom.nasa.gov) (Block 1c of Figure 6.5).

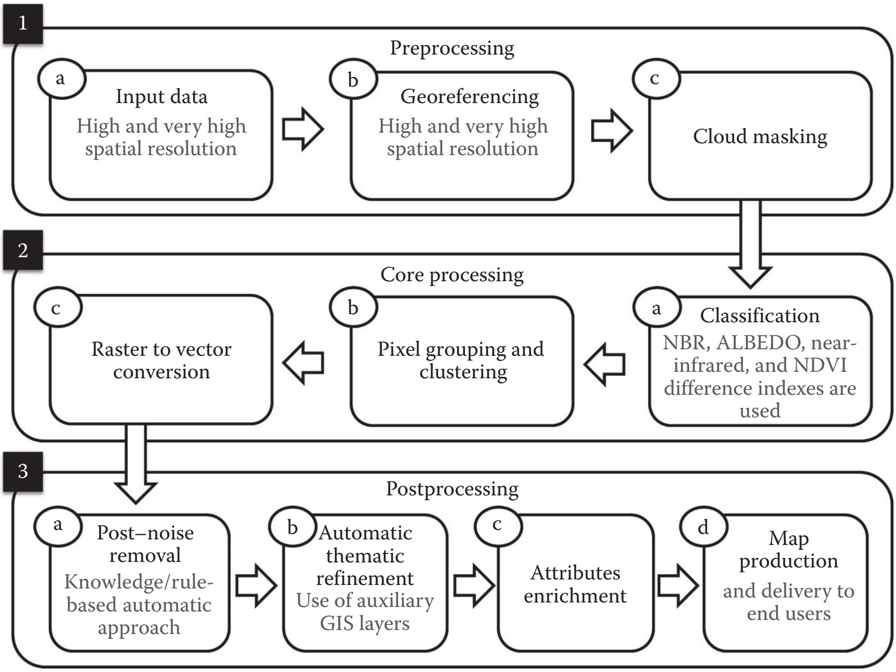

FIGURE 6.5
The FireHub BSM-NOA service chain.

2. The core processing stage:

The focus on the core processing phase is the burnt area classification algorithm (Block 2a of Figure 6.5). The algorithm aims at identifying burnt and nonburnt sets of pixels within the georeferenced satellite image. Each image pixel is basically a vector of intensities that correspond to emissions from different frequency channels. Using the Landsat 5 TM as an example, a raw image consists of seven spectral bands. Classification to burnt and nonburnt areas relies on the fact that the emissions from different frequency bands have a physical interpretation. Simple band algebra can lead to the derivation of physical indexes. The main criteria used within the BSM-NOA process to correctly classify pixels are as follows: (1) the Normalised Burn Ratio (NBR) Index, (2) the Albedo Index, (3) the Normalized Difference Vegetation Index (NDVI), and (4) the $NDVI_{MULTI}$, which is the difference of the two NDVIs calculated before and after a fire event over the same area. Then, a decision tree is formed where the adopted indexes are compared to site-specific thresholds. These image indexes are as follows:

a. *The NBR*: It is one of the most widely used image enhancements for mapping wildfires worldwide. Key and Benson (2003) introduced this index as a variation of the NDVI. They replaced the red reflectance value in the NDVI with the mid-infrared reflectance value:

$$\mathrm{NBR} = \frac{(R_{\mathrm{NIR}} - R_{\mathrm{MIR}})}{R_{\mathrm{NIR}} + R_{\mathrm{MIR}}} \tag{6.2}$$

with R_{NIR} and R_{MIR} denoting the reflectance values recorded in the NIR and mid-infrared channels of the satellite image (Bands 4 and 7 of Landsat TM), respectively.

Several researchers have proposed this index for burnt area mapping (Cocke et al. 2005; Roy et al. 2006), as reflectance values in the red and mid-infrared ranges exhibit the greatest reflectance change in response to a fire. Although NBR has been effective in many burnt areas mapping studies, it has not been widely tested for Greek ecosystems. In the south Mediterranean zones and especially within the Greek pine and shrubland ecosystems, land abandonment has resulted in intense fuel accumulation. Because of this, a significant reduction in green vegetation is reported inside the burnt areas after a fire occurrence. In these areas, the NBR index can differentiate accurately between burnt and unburnt areas. Forest ecosystems, however, are much diversified in Greece and forest canopy density decreases from north to south. Therefore, the forest stands become less uniform and are interrupted by the presence of agricultural fields, dispersed settlements, roads, open fields, abandoned farms, or permanent crop cover. This high mixture of classes makes automatic image segmentation with the sole use of NBR problematic. Indeed, because the burnt vegetation is characterized by an increase in reflectance in the VIS, a decrease in the NIR, and a slight increase in the mid-infrared, the spectral response of burnt forests tends to be "flatter" than that of healthy vegetation, which may cause confusion with nonvegetation classes like open agricultural fields, bare soils, water surfaces, urban areas, or permanent crops. This type of confusion between charcoal and other soil colors in highly fragmented ecosystems was also reported by Rogan and Yool (2001), who suggested the use of the Kauth–Thomas tasselled cap transformation (Kauth and Thomas 1976) to resolve the reported confusion. In order to cope with this problem, the BSM-NOA approach integrates two additional spectral indices complementary to NBR.

b. *The uni- or multitemporal NDVI (NDVI and $NDVI_{MULTI}$)*: The NDVI is a common spectral vegetation index derived by dividing the difference between reflectance in the NIR and the VIS red channels by the sum of the two (Rouse et al. 1974):

$$\mathrm{NDVI} = \frac{(R_{\mathrm{NIR}} - R_{\mathrm{RED}})}{R_{\mathrm{NIR}} + R_{\mathrm{RED}}} \tag{6.3}$$

with R_{NIR} and R_{RED} denoting the reflectance values recorded in the NIR and red channels of the multispectral satellite image, respectively.

NDVI has long been used in the Mediterranean for assessing the vegetative health and moisture content of an area and resolving ambiguities in the discrimination between healthy and dead or removed vegetation (Marsh et al. 1992; Tappan et al. 1992; Lyon et al. 1998). Moreover, NDVI has been used to demonstrate the extent of vegetation removal associated with a fire event, as it exhibits a sharp postfire drop (Li et al. 2000; Diaz-Delgado and Pons 2001; Vafeides and Drake 2005). Depending on the number of acquisitions, the NDVI analysis can be unitemporal (calculated only at the postfire level) or multitemporal. The multitemporal difference of NDVI adopted in BSM-NOA is denoted as $\mathrm{NDVI}_{\mathrm{MULTI}}$ and is calculated using the following equation:

$$\mathrm{NDVI}_{\mathrm{MULTI}} = \mathrm{NDVI}_{\mathrm{PREFIRE}} - \mathrm{NDVI}_{\mathrm{POSTFIRE}} \tag{6.4}$$

with $\mathrm{NDVI}_{\mathrm{PREFIRE}}$ and $\mathrm{NDVI}_{\mathrm{POSTFIRE}}$ denoting the NDVI values calculated before and after a fire occurrence over the affected area, respectively.

The multitemporal NDVI approach is preferred to a unitemporal one, as it better resolves the confusion between classes. Several studies have differenced prefire and postfire NDVI images to discern fire scars fast and efficiently (Cahoon et al. 1992; Kasischke et al. 1993; Kasischke and French 1995; Li et al. 1997; Leblon et al. 2001).

c. *The albedo index*: In highly diversified Mediterranean ecosystems, the NDVI might put limitations on the detection and delineation of burnt from unburnt surfaces. Pereira (1999) and Elmore et al. (2000) concluded that the NDVI is affected by soil color and is therefore not always comparable across a heterogeneous area. Due to this issue, BSM-NOA integrates the empirical approximation of the surface albedo (Saunders 1990; Lasaponara 2006), which is an indicator of the surface brightness. The albedo index is calculated using the following equation:

$$\mathrm{ALBEDO} = \frac{R_{\mathrm{NIR}} + R_{\mathrm{RED}}}{2} \tag{6.5}$$

with R_{NIR} and R_{RED} denoting the reflectance values recorded in the NIR and red channels of the multispectral satellite image, respectively.

From the above, it is shown that none of the proposed image indexes by themselves can be considered sufficient to efficiently resolve the problem of burnt area mapping in south Mediterranean ecosystems. Hence, the BSM-NOA approach suggests the appropriate thresholding and combined use of the three image indexes, with appropriate classification refinement (noise removal) processes, which is performed at the postprocessing level (Kontoes et al. 2009).

Upon deciding on the burnt and nonburnt pixels of the image, the neighboring pixels are grouped together (Block 2b of Figure 6.5) since they constitute the same fire event, and then the raster is converted to vector (ESRI polygons) (Block 2c of Figure 6.5) to proceed to the postprocessing phase (Figure 6.5).

3. The postprocessing stage:

   a. Noise removal, the process necessary to eliminate isolated pixels that have been wrongfully classified as burnt. The minimum mapping unit depends on the spatial resolution of the input satellite data and ranges from 0.5 to 1 ha. Hence, a rectangle group of pixels with an edge of three or fewer pixels (for the case of Landsat TM with 30-m spatial resolution) should not be classified as burnt. This filtering is performed with the appropriate spatial functions using the Geospatial Data Abstraction Library *via* the Python programming language API (Application Programming Interface) (Block 3a of Figure 6.5).

   b. In addition, a set of logical classification rules is applied, using evidence from a series of auxiliary GIS layers, to ensure product thematic accuracy and consistency with the underlying land use/land cover conditions and landscape morphology. The basic operations performed are (1) refinement of the polygons to comply with certain restrictions, similar to those applicable for the fire monitoring scenario (burnt areas in the sea, or inconsistent underlying land cover types) and (2) normal GIS processes such as classification polygon aggregation and polygon boundary smoothing. The final refinement stage relies on the employment of visual checks to resolve any remaining classification inconsistencies and uncertainties. The aforementioned approach was developed to minimize any manual (visual interpretations) operations that are laborious and time consuming (Block 3b of Figure 6.5).

   c. Attribute enrichment of the BSM product by overlaying the polygons with geoinformation layers (e.g., Greek Administrative Geography, CLC, open data, etc.) (Block 3c of Figure 6.5).

d. Generation of thematic maps that include damage assessments, that is, the land cover types and quantities of burnt areas per prefecture, at a national level (Block 3d of Figure 6.5).

Figure 6.6 provides a more detailed view of the main algorithmic step of the BSM-NOA approach, based on multidate (prefire and postfire) image acquisition to generate burnt scar maps in vector and raster format.

The BSM product is ideal for use in further environmental time series analyses, production of statistical indexes (frequency of fire occurrence, geographical distribution, and number of fires over the studied territory) and applications, including change detection and climate change models, urban planning, and correlation with manmade activities. The BSM-NOA service is freely provided through the FireHub platform, allowing end users to search, view and retrieve (1) the annual BSM records at a fully detailed scale, (2) a single map layer depicting the areas affected for the last 30 years, (3) the number of times a certain area has been affected by fires, and (4) information and statistics on the impact of forest fires on the natural and built environment at the prefecture, regional, and country levels.

Figure 6.7 shows cases of BSMs and damage assessments derived for selected wildfires in Greece during recent years.

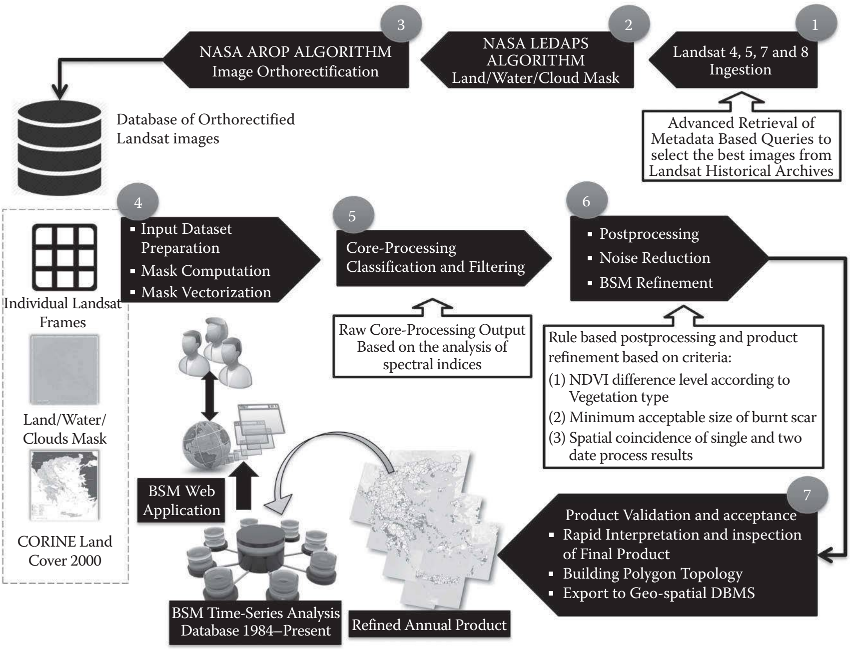

FIGURE 6.6
BSM-NOA algorithmic workflow.

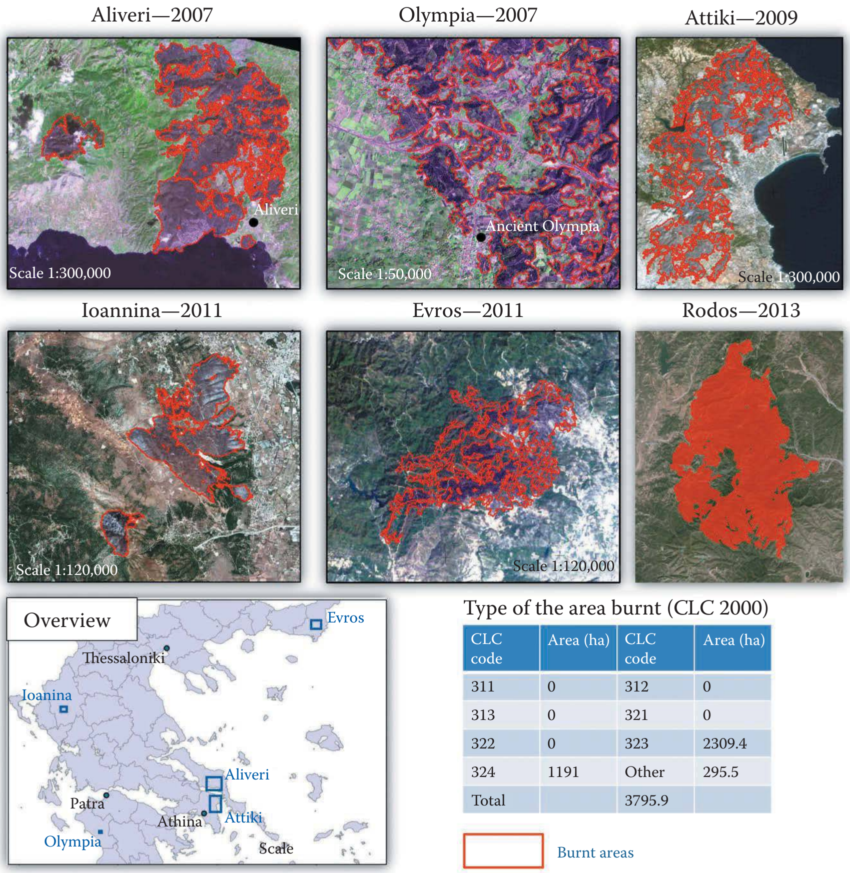

Type of the area burnt (CLC 2000)

CLC code	Area (ha)	CLC code	Area (ha)
311	0	312	0
313	0	321	0
322	0	323	2309.4
324	1191	Other	295.5
Total		3795.9	

FIGURE 6.7
Selected cases of BSM-NOA mapping and damage assessments over Greece.

Evaluation of Fire Products and Services

Real-Time Fire Monitoring Service

During the summer of 2013, active fire occurrence data were collected in order to validate the fire detection process. The data attributes taken under consideration were as follows: (1) fire locations (at the commune level), (2) ignition time (first alarm), (3) time of first intervention by the fire brigade, (4) burnt area type (forest and nonforest), and (5) burnt area in hectares per area type. These data were found in reports provided by the Hellenic Fire Brigade on a daily basis. The information regarding the area burnt and the burnt area type were *ad hoc* estimations provided by firefighters, submitted during or after suppression of the active fire event. For cross-validation purposes, additional information from the local media was taken under consideration. The evaluation process entailed the matching of active fire events recorded in the reports with the data returned by the hotspot detection algorithm delivered every 5 minutes.

The approach focuses on evaluating the fire detection accuracy of the algorithm as a percentage of the events obtained from the fire brigade that were also successfully detected by the algorithm. Additionally, the capability of the algorithm to provide early warnings about fire events was investigated, by comparing the ignition time provided by the algorithm with the ignition time provided by the fire brigade. To estimate the algorithm's performance concerning the fire's location in real time, the active hotspots returned by the algorithm within the 500 × 500 m wide cells were compared with the BSM polygons, the latter referring to the entire fire season over Greek territory. The BSM polygons used as reference were generated from the full Landsat TM data set acquired over Greece immediately after the end of the fire season 2013. Due to the much higher spatial resolution of the Landsat TM data compared to the MSG/SEVIRI-based fire detections, the derived BSM polygons were considered an ideal validation data set to assess the fire detection algorithm's robustness. Therefore, the accuracy of the MSG/SEVIRI active fire detection was assessed through the estimation of the commission error, that is, returned as hotspots by the MSG/SEVIRI processing chain but not included in the BSM polygons, and the omission error, that is, the number of hotspot locations from the reports included in the BSM polygon but not returned by the MSG/SEVIRI-based algorithm outputs.

Table 6.1 presents a comparison between the total BSM area and the area that was successfully detected by the real-time MSG/SEVIRI-based wildfire detection algorithm. Ninety-three percent of the burnt areas' surface mapped over the entire country matches with the returned MSG/SEVIRI-based fire polygons detected, and only a percentage of 7% of the burnt areas was missed.

An additional criterion for assessing the algorithm's accuracy is shown in Table 6.2. This table represents the number of fire events reported by the fire brigade log files (Column 2 of Table 6.2) that were successfully matched with the returned active fire detections (Column 3 of Table 6.2) in relation to the size of the affected area.

TABLE 6.1

Comparison of the BSM Total Area, with the BSM Area Detected by the MSG/SEVIRI Wildfire Detection Algorithm at National Scale

	Area Size (ha)
Nationwide *BSM* area as mapped from the Landsat TM imagery (*BSM-NOA*)	20,100
Nationwide *BSM* area returned by the MSG/SEVIRI-based real-time detection algorithm	18,727 (93%)
Nationwide omitted *BSM* area not returned by the MSG/SEVIRI-based real-time detection algorithm	1,373 (7%)

TABLE 6.2

Comparison of the Reported Fire Events in the Fire Brigades Log Files, with the Active Fire Events Returned by the MSG/SEVIRI Forest Fire Detection Algorithm

Affected Area (ha)	Total Fire Events (Fire Service)	Reported by Fire Brigades and Matched by MSG/SEVIRI	Level of Matching (%)
0–50	57	18	32
50–100	12	9	75
100–150	3	3	100
150–200	4	4	100
≥200	11	11	100
Summary	87	45	52

Smaller size fires, with active burning areas of less than 50 ha, could not be detected by the system with adequate accuracy. This is because the fire radiation emitted is not at the required level to saturate the corresponding low spatial resolution MSG/SEVIRI pixel. Another reason relates to the fact that the fire detection system has an internal control mechanism, which returns a first fire occurrence only after it has been detected in two out of the three consecutive observations. Therefore, for small fires that are rapidly controlled by the firefighting mechanism, that is, within the first 15–30 minutes, there is not enough time for the system to confirm that its first detections match with the subsequent two to three observations. This control mechanism prevents the system from sending fire alarms to the fire brigades that are not certain.

Thus, for the above reasons the detection efficiency of the system for small fires is limited to the order of 32%. However, as shown in Table 6.2, larger fire events with sizes greater than 50 ha were adequately detected by the system with a level of accuracy ranging between 75% and 100%. There are two main reasons for the omitted detections: the first one relates to the presence of sparse clouds in the field of view of the sensor, while the second is because, for a few cases, the algorithm thresholds were not appropriate to detect the wildfire. However, lowering the thresholds would lead to increasing the false alarm rate; as expected, there is always a trade-off between false positives and false negatives.

To evaluate the capability of the real-time detection process to timely detect a fire event, the first fire alarm returned by the system was compared with the ignition time provided in the fire brigade log files. Table 6.3 summarizes the outcome of this validation. Out of the total of 45 fire events used for validation, 7 were first detected earlier than their announcement from the fire brigade control room. For the remaining events, 11 were detected with a delay of 0–15 minutes, 6 with a delay of 15–30 minutes, and 18 with a delay of 30–45 minutes.

TABLE 6.3

Comparison of the Time an Event Was First Detected by the Forest Fire Detection Algorithm with the Time Given by the Fire Brigades Service Report

Time Difference (minutes)	Number of Events
–15, 0	7
0, 15	11
15, 30	6
30, 45	18

BSM-NOA Service

The entire BSM-NOA service chain was extensively evaluated by subjecting it to a standardization procedure using several criteria (thematic accuracy, user support, sustainability of the means used, transferability, timeliness, etc.). The validation was done in the framework of the RISK-EOS/ESA/GSE and SAFER EC/GMES projects, which aimed to establish qualified and validated emergency response and emergency support services based on EO technology to meet the operational needs of the end-user communities. The validation experiments were internal in NOA and external from the Joint Research Centre, using high accuracy reference data over various European test sites (Greece, Portugal, Spain, and Corse). Scientific and technical validation of the product was carried out both in terms of vector data and map layout. The validation experiments compared the service BSM-NOA products against ground-truth data, the latter generated through dedicated *in situ* field campaigns. The surface accuracy figures are expressed in terms of detected area efficiency, skipped area rate (omission error), and false area rate (commission error). These accuracy figures were calculated on the basis of the following formulae:

$$\text{Detected area efficiency} = \frac{\text{DBA}}{\text{DBA} + \text{SBA}} \tag{6.6}$$

$$\text{Commission error } \left(\text{flase area rate}\right) = \frac{\text{FBA}}{\text{DBA} + \text{FBA}} \tag{6.7}$$

$$\text{Ommission error } \left(\text{skipped area rate}\right) = \frac{\text{SBA}}{\text{DBA} + \text{SBA}} \tag{6.8}$$

where DBA is the detected burnt area (common area between the generated burn scar polygon and the reference *in situ* polygon), FBA is the false burnt area (area included in the generated burn scar polygon but not in the reference *in situ* polygon), and SBA is the skipped burnt area (area included in the reference *in situ* polygon but not in the generated burn scar polygon).

The results of the validation experiments showed that the BSM-NOA service, and its subsequent evolution as a module of the NOA FireHub platform, is capable of processing images with different spectral and spatial resolutions and can effectively exploit data from different acquisition modes (uni- and multitemporal). In a multitemporal approach using a pair of Landsat 5 TM images, the method performed better than using a single-date image in identifying the postfire decrease of vegetation vigor and minimizing the spectral confusion of burnt areas with classes such as permanent crops, bare soil, shadows, urban fabric, and water. The minimum burnt area size detected is approximately 0.9–1.0 ha nonetheless, and the method performs well in delineating small fires of ~0.8–2.5 ha located in the alpine zones of the Mediterranean mountains.

The overall burnt area detection accuracy returned in the different evaluation experiments conducted reached levels of 85%–91%, with omission errors at the level of 9%–15% and commission errors as low as 6%–4% (Kontoes et al. 2013a). In fact, the service was qualified in the framework of the SAFER EC/GMES project—top of its class—as an end-to-end service for fire-related emergency support activities for integration into operational scenarios all over Europe. Figure 6.8 illustrates the BSM polygons for the Penteli Mt (2007)

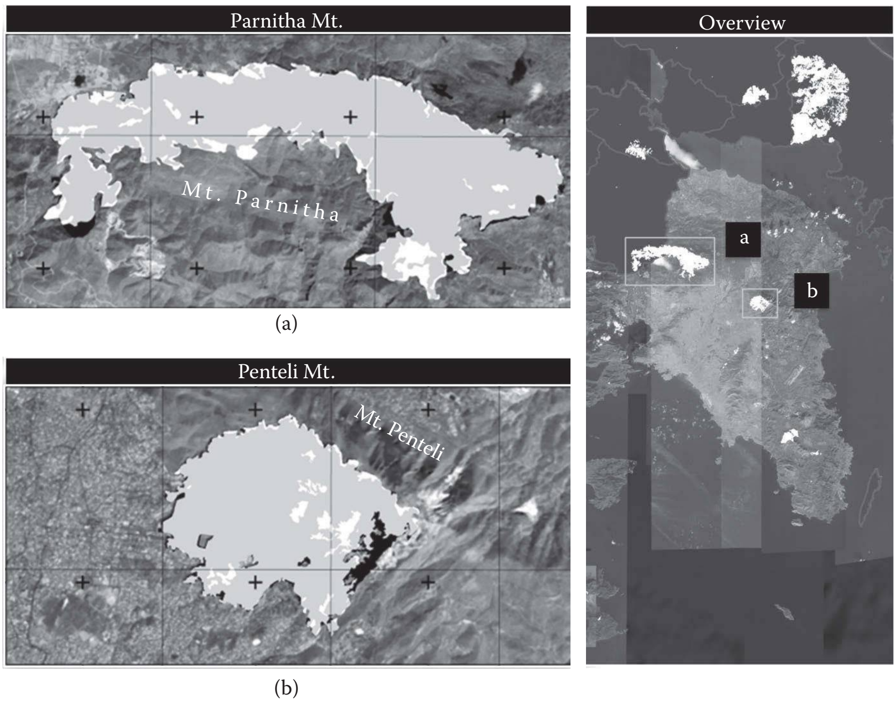

FIGURE 6.8
Burn scar mapping in the Mt. Parnitha and Penteli Mt. fires using the BSM-NOA method.

and Mount Parnitha (2007) fires in Greece, as well the omission (white areas) and the commission errors (black areas) reported with respect to the reference validation data used (Kontoes et al. 2009).

Discussion and Conclusions

The application of the MSG/SEVIRI active fire detection methodology over Greece has provided objective and accurate detections of wildfire spots with satisfactory accuracy on a 5-minute basis. The reported results provide insights into the method's flexibility, timeliness, and efficiency, especially when applied to very large areas that extend beyond the national scale. Moreover, the active fire maps generated when used in combination with highly accurate fuel maps can provide a useful overall fire situation awareness picture for the effective deployment of fire suppression resources and promoting evidence-based decision-making.

Based on the specific end-user demands, the fire detection algorithm was expanded further during the development of the FireHub platform operated by NOA's BEYOND Center of Excellence for EO-based monitoring and management of natural disaster. This patent-pending approach results in a subpixel approximation (500 × 500 m wide) of wildfire presence within the initial MSG/SEVIRI pixel. Several elements and information layers were taken under consideration to achieve such a level of precision. A sophisticated data fusion approximation is used, combining satellite fire detections with updated fuel data and fire spread models using real-time weather information. The hotspot detection methodology was assessed against reference information on real cases of fire events, with the conclusion of accurate fire estimation, with certain restrictions when it comes to small fire events.

According to the feedback received from the fire brigade and civil protection authorities, the FireHub approach with its enhanced spatial resolution is exceeding the EO-based real-time active hotspot detection standards established by the fire and forestry bodies for supporting actions relating to wildfire suppression management. Following the Copernicus (GMES) standards, the method is characterized by high flexibility and transferability; that is, it is applicable to other geographic areas in Europe, featuring an interactive approach for the definition and fine tuning of the spectral thresholds for active fire spot detection. Moreover, the dynamic integration of medium resolution satellite images that are acquired every 2–3 hours at the NOA reception stations, such as NOAA/AVHRR, MODIS, Suomi NPP, and MetOp, can update the hotspot products derived from the MSG/SEVIRI low spatial but high temporal resolution sensor, constituting a suitable and robust solution for operational active fire monitoring at the European, national, and regional levels.

This chapter also provided concrete evidence that the NOA's FireHub platform offers advanced burnt area mapping capabilities to meet rush and nonrush fire mapping needs for emergency response, emergency support, and recovery operations at the regional, national, or continental levels. It requires limited effort from an operator and returns higher mapping accuracies, compared to conventional mapping approaches (e.g., field surveys, aerial photo interpretation, GPS campaigns, etc.), as shown by Kontoes et al. (2009). The mapping accuracy of the developed remote sensing method was assessed in a very challenging environment, namely the accentuated relief and highly diversified ecosystems of the mountainous terrain of Greece. The approach proved highly sensitive in detecting burnt areas and avoiding spectral confusion with other classes such as bare soil, urban fabric, water, and permanent crops. Finally, the methodologies presented here, as well as the overall experience gained through several Copernicus (GMES) projects, suggest that the satellite-based mapping methods can certainly replace previous mapping methods, providing accuracies that exceed the end-user's operational requirements.

The NOA Web services (fire detection and monitoring, as well as BSM-NOA) and the generated products are delivered to institutional end users (e.g., Hellenic Fire Brigade, General Secretariat of Civil Protection, Copernicus EMS, Forestry Services, etc.) and are now part of the everyday decision-making processes of these institutions. As such, the FireHub platform was awarded first prize for Best Challenge Service in the Copernicus Masters Competition of 2014.

Acknowledgments

The research mentioned in this chapter and the relevant results were supported by the following European Community and ESA projects:

1. BEYOND—Building a Centre of Excellence for Earth Observation–Based Monitoring of Natural Disasters in Southeastern Europe, EC Seventh Framework Programme (FP7-REGPOT-2012-2013-1), Grant Agreement 316210.
2. SAFER—Services and Applications for Emergency Support. Program for Global Monitoring for Environment and Security (GMES)/EC/FP7-2007-SPACE-1/GMES Collaborative Project. Grant Agreement 218802.
3. TELEIOS—Virtual Observatory Infrastructure for Earth Observation Data. Program FP7-ICT-2009-5 Collaborative Project. Grant Agreement 257662.

4. RISK-EOS Extension to Greece—Promotion of the GSE RISK-EOS fire services portfolio in Greece. Program for Global Monitoring for Environment and Security. Service Consolidation Actions of EarthWatch GMES Services Elements, ESA/GSE Program. Contract Notice: Ref. ITF-Aj-0043-08.

We are grateful to Dr Ioannis Mitsopoulos for his support and effort in reviewing the manuscript and providing valuable comments raising the scientific value of the chapter.

References

Amraoui, M., DaCamara, C., and J. Pereira. 2010. Detection and monitoring of African vegetation fires using MSG-SEVIRI imagery. *Remote Sensing of Environment* 114: 1038–1052.

Amraoui, M., Liberato, M., Calado, T., DaCamara, C., Coelho, L., Trigo, R., and C. Gouveia. 2013. Fire activity over Mediterranean Europe based on information from Meteosat-8. *Forest Ecology and Management* 294: 62–75.

Arino, O., Piccolini, I., Siegert, F., et al. 1999. Burn scars mapping methods, forest fire monitoring and mapping: A component of global observation of forest cover. In *Report of a Workshop*, F. Abern, J-M. Gregoire and C. Justice (eds.), Joint Research Centre, Ispra, Italy, pp. 198–223.

Bassi, S., Kettunen, M., Kampa, E., and S. Cavalieri. 2008. Forest fires: Causes and contributing factors in Europe; IP/A/ENVI/ST/2007-15 PE 401.003; Policy Department, Economic and Scientific Policy, European Parliament, Brussels, Belgium.

Brieb, K., Jahn, H., Ginati, A., and K. Sommer. 1996. A small satellite solution for the fire detection and monitoring from space. *Acta Astronautica* 39: 447–457.

Cahoon, D., Stocks, B., Levine, J., Cofer, W., and C. Chung. 1992. Evaluation of a technique for satellite-derived area estimation of forest fires. *Journal of Geophysical Research* 97: 3805–3814.

Calle, A., Casanova, J., and A. Romo. 2006. Fire detection and monitoring using MSG spinning enhanced visible and infrared imager (SEVIRI) data. *Journal of Geophysical Research* 111: G04S06.

Chuvieco, E., and M. Martin. 1994. A simple method for fire growth mapping using AVHRR channel 3 data. *International Journal of Remote Sensing* 15: 3141–3146.

Chuvieco, E., Martin, M. P., and A. Palacios. 2002. Assessment of different spectral indices in the red near-infrared spectral domain for burned land discrimination. *International Journal of Remote Sensing* 23(16): 5103–5110.

Cocke, A. E., Fule, P. Z., and J. E. Crouse. 2005. Comparison of burn severity assessments using differenced normalized burn ratio and ground data. *International Journal of Wildland Fire* 14(2): 189–198.

Collins, J. B., and C. E. Woodcock. 1996. An assessment of several linear change detection techniques for mapping forest mortality using multitemporal LandsatTM data. *Remote Sensing of Environment* 56: 66–77.

Diaz-Delgado, R., and X. Pons. 2001. Spatial patterns of forest fires in Catalonia (NE of Spain) along the period 1975–1995. Analysis of vegetation recovery after fire. *Forest Ecology and Management* 147: 67–74.

Dimitrakopoulos, A., and I. Mitsopoulos. 2005. Thematic report on forest fires in the Mediterranean Region. Forest Fire Management Working Paper 8, FAO. In *Global Forest Resources Assessment, 2005*, A.P. Vuorinen (ed.), 43 p.

Dimitrakopoulos, A., Vlahou, M., Anagnostopoulou, Ch., and I. Mitsopoulos. 2011. Impact of drought on wildland fires in Greece; Implications of climatic change? *Climate Change* 109: 331–347.

Elmore, A. J., Mustard, J. F., Manning, S. J., and D. B. Lobell. 2000. Quantifying vegetation change in semiarid environments: Precision and accuracy of spectral mixture analysis and the normalized difference vegetation index. *Remote Sensing of Environment* 73: 87–102.

Finney, M. 2002. Fire growth using minimum travel time methods. *Canadian Journal of Forest Research* 32: 1420–1424.

Finney, M. 2006. An overview of FlamMap modeling capabilities. In *Fuels Management - How to Measure Success: Conference Proceedings*, USDA, Forest Service, Rocky Mountain Research Station, General Technical Report, RMRS-P-41, P. Andrews, and B. Butler (eds.), pp. 213–219.

Fisher, R., Vigilante, T., Yates, C., and J. Russel-Smith. 2003. Patterns of landscape fire and predicted vegetation response in the North Kimberley region of Western Australia. *International Journal of Wildland Fire* 12(3–4): 369–379.

Fraser, R. H., and Z. Li. 2002. Estimating fire related parameters in boreal forests using SPOT VEGETATION. *Remote Sensing of Environment* 82: 95–110.

Fung, T., and C. Y. Jim. 1998. Assessing and modelling hill fire impact in country parks with SPOT HRV images and GIS. *Geocarto International* 13(1): 47–58.

Gao, F., Masek, J., and R. E. Wolfe. 2009. Automated registration and orthorectification package for Landsat and Landsat-like data processing. *Journal of Applied Remote Sensing* 3(1): 033515.

Giannakopoulos, C., Le Sager, P., Bindi, M., Moriondo, M., Kostopoulou, E., and C. Goodess. 2009. Climatic changes and associated impacts in the Mediterranean resulting from a 2° C global warming. *Global Planetary Change* 68: 209–224.

Giglio, L., Descloitres, J., Justice, C., and Y. Kaufman, 2003. An enhanced contextual fire detection algorithm for MODIS. *Remote Sensing of Environment* 87: 273–282.

Gong, P., Pu, R., Li, Z., Scarborough, J., Clinton, N., and L. M. Levien. 2006. An integrated approach to wildland fire mapping of California, USA using NOAA/AVHRR data. *Photogrammetric Engineering and Remote Sensing* 72(2): 139–150.

Justice, C., Giglio, L., Korontzi, S., et al. 2002. The MODIS fire product. *Remote Sensing of Environment* 83: 244–262.

Kasischke, E., and H. French. 1995. Locating and estimating the areal extent of wildfires in Alaskan Boreal Forest, using multiple season AVHRR NDVI composite data. *Remote Sensing of Environment* 51: 263–275.

Kasischke, E., French, H., Harrell, P., Christensen, N., Ustin, S., and D. Barry. 1993. Monitoring of wildfires in Boreal forests using large area AVHRR NDVI composite image data. *Remote Sensing of Environment* 45: 61–71.

Kaufman, J., Justice, C., Flynn, L., et al. 1998. Potential global fire monitoring from EOS-MODIS. *Journal of Geophysical Research* 103: 32215–32238.

Kauth, R., and G. Thomas. 1976. The Tasseled Cap—A graphic description of the spectral–temporal development of agricultural crops as seen by Landsat.

Proceedings of the Symposium on Machine Processing of Remotely Sensed Data, Purdue University, West Lafayette, IN, pp. 41–51.

Key, C., and N. C. Benson. 2003. *The Normalised Burn Ratio (NBR): A Landsat TM radiometric measure for burn severity*. http://www.nrmsc.usgs.gov/research/ndbr.html

Kontoes, C., Keramitsoglou, I., Papoutsis, I., Sifakis, N., and P. Xofis. 2013a. National scale operational mapping of burnt areas as a tool for the effective development of wildfire management strategy. *Sensors* 18: 11146–11166.

Kontoes, C. C., Poilvé, H., Florsch, G., Keramitsoglou, I., and S. Paralikidis. 2009. A comparative analysis of a fixed thresholding vs. A classification tree approach for operational burn scar detection and mapping. *International Journal of Applied Earth Observation and Geoinformation* 11(5): 299–316. ISSN 0303 2434, DOI: 10.1016/j.jag.2009.04.00.

Koubarakis, M., Kyzirakos, K., Karpathiotakis, M., et al. 2012. TELEIOS: A database-powered virtual earth observatory. In *Proceedings of International Conference on Very Large Data Bases 2012, 38th International Conference on Very Large Databases (VLDB 2012)*.

Koutsias, N. 2000. Burned area mapping using logistic regression modelling of a single post-fire Landsat-5 Thematic Mapper image. *International Journal of Remote Sensing* 21(4): 673–687.

Koutsias, N., and M. Karteris. 2000. Burned area mapping using logistic regression modeling of a single post-fire Landsat-5 Thematic Mapper image. *International Journal of Remote Sensing* 21(4): 673–687.

Koutsias, N., Xanthopoulos, G., Founda, D., et al. 2013. On the relationships between forest fires and weather conditions in Greece from long-term national observations (1894–2010). *International Journal of Wildland Fire* 22: 493–507.

Kyzirakos, K., Karpathiotakis, M., and G. Garbis. 2014. Wildfire monitoring using satellite images, ontologies and linked geospatial data. *Journal of Web Semantics* 24: 18–26, DOI: 10.1016/j.websem.2013.12.002.

Kyzirakos, K., Karpathiotakis, M., Garbis G., et al. 2012. Real Time fire monitoring using semantic web and linked data technologies. *Presented in the 11th International Semantic Web Conference*. Boston, MA. November 11–15, 2012.

Laneve, G., Castronuovo, M., and G. Cadau. 2006. Continuous monitoring of forest fires in Mediterranean Area using MSG. *IEEE Transactions on Geoscience and Remote Sensing* 44: 2761–2768.

Lasaponara, R. 2006. Estimating spectral separability of satellite derived parameters for burned areas mapping in the Calabria region by using SPOT-Vegetation data. *Ecological Modelling* 196(1–2): 265–270.

Leblon, B., Alexander, M., Chen, J., and S. White. 2001. Monitoring fire danger of Northern Boreal Forests with NOAA-AVHRR NDVI images. *International Journal of Remote Sensing* 22(14): 2839–2846.

Li, Z., Cilar, J., Moreau, L., Huang, F., and B. Lee. 1997. Monitoring fire activities in the Boreal ecosystem. *Journal of Geophysical Research* 102: 29611–29624.

Li, Z., Kaufman, Y. J., Ichku, C., Fraser, R., Trishchekno, A., Giglio, L., Jin, J., and X. Yu. 2001. A review of AVHRR-based active fire detection algorithms: Principles, limitations, and recommendations. In *Global and Regional Vegetation Fire Monitoring from Space: Planning and Coordinated International Effort*. A. Abern., J. G. Goldammer and C. Justice (eds.), SPB Academic Pub., The Hague, The Nederlands, pp. 199–225.

Li, Z., Nadon, S., and J. Cihlar. 2000. Satellite detection of Canadian boreal forest fires: Development and application of the algorithm. *International Journal of Remote Sensing* 21: 3057–3069.

Lyon, G. J., Ding, Y., Lunetta, R. S., and C. D. Elvidge. 1998. A change detection experiment using vegetation indices. *Photogrammetric Engineering and Remote Sensing* 64(2): 143–150.

Marsh, S., Walsh, J., Lee, C., Beck, L., and C. Hutchinson. 1992. Comparison of multi-temporal NOAA-AVHRR and SPOT XS satellite data for mapping land cover dynamics in the West African Sahel. *International Journal of Remote Sensing* 13: 2997–3016.

Martin, M. P., and E. Chuvieco. 1995. Mapping and evaluation of burnt land from multi-temporal analysis of AVHRR NDVI images. *EARSEL Advance Remote Sensing* 4: 7–13.

Miller, J. D., and S. R. Yool. 2002. Mapping forest post-fire canopy consumption in several overstory types using multi-temporal Landsat TM and ETM data. *Remote Sensing of Environment* 82: 481–496.

Pennypacker, C., Jakubowski, M., Kelly, M., et al. 2013. FUEGO—Fire Urgency Estimator in Geosynchronous Orbit—A proposed early-warning fire detection system. *Remote Sensing* 5: 5173–5192.

Pereira, J. M. C. 1999. A comparative evaluation of NOAA/AVHRR vegetation indexes for burned surface detection and mapping. *IEEE Transactions on Geoscience and Remote Sensing* 37: 217–226.

Prins, E. M., and W. P. Menzel. 1996. *Investigation of biomass burning and aerosol loading and transport utilizing geostationary satellite data*. Biomass and Global Change, MIT Press, Cambridge, MA, pp. 67–72.

Prins, E. M., Schmidt, C. C., Feltz, J. M., Reid, J. S., Wesphal, D.L., and Richardson, K. 2003. A two year analysis of fire activity in the Western Hemisphere as observed with the GOES Wildfire Automated Biomass Burning Algorithm. *Preprints, 12th Conf. on Satellite Meteorology and Oceanography, Long Beach, CA, Amer. Meteor. Soc.*, CD-ROM, p. 2.28

Pu, R., and P. Gong. 2004. Determination of burnt scars using logistic regression and neural network techniques from single post-fire Landsat 7 ETM+ image. *Photogrammetric Engineering and Remote Sensing* 70(7): 841–850.

Quintano, C., Fernandez-Manso, A., Fernandez-Manso, O., and Y.E. Shimabukuro. 2006. Mapping burned areas in Mediterranean countries using spectral mixture analysis from a uni-temporal perspective. *International Journal of Remote Sensing* 27(4): 645–662.

Roberts, G., and M. Wooster. 2008. Fire detection and fire characterization over Africa using Meteosat SEVIRI. *IEEE Transactions on Geoscience and Remote Sensing* 46: 1200–1218.

Rogan, J., and S. Yool. 2001. Mapping fire induced vegetation depletion in the Peloncillo Mountains, Arizona and New Mexico. *International Journal of Remote Sensing* 22(16): 3101–3121.

Rouse, J.W., Haas, R.H., Schell, J.A., and Deering, D.W. 1974. Monitoring vegetation systems in the Great Plains with ERTS. In: S.C. Freden, E.P. Mercanti, and M. Becker (eds) *Third Earth Resources Technology Satellite–1 Syposium. Volume I: Technical Presentations*, NASA SP-351, NASA, Washington, DC, pp. 309–317.

Roy, D. R., Boscheti, L., and S. N. Trigg. 2006. Remote sensing of fire severity: Assessing the performance of the normalized burn ratio. *IEEE Geoscience and Remote Sensing Letters* 3(1): 112–116.

Sa, A. C. L., Pereira, J. M. C., Vasconcellos, M. J. P., Silva, J. M. N., Ribeiro, N., and A. Awasse. 2003. Assessing the feasibility of sub-pixel burned area mapping in miombo woodlands of northern Mozambique using MODIS imager. *International Journal of Remote Sensing* 24: 1783–1796.

San-Miguel-Ayanz, J., Ravail, N., Kelha, V., and A. Oller. 2005. Active fire detection for fire emergency management: Potential and limitations for the operational use of remote sensing. *Natural Hazards* 35: 361–376.

Saunders, R. W. 1990. The determination of broad band surface albedo from AVHRR visible and near-infrared radiances. *International Journal of Remote Sensing* 11(1): 49–67.

Sifakis, N., Iossifidis, C., Kontoes, C., and I. Keramitsoglou. 2011. Wildfire detection and tracking over Greece using MSG-SEVIRI satellite data. *Remote Sensing* 3: 524–538.

Sifakis N., Paronis D., and I. Keramitsoglou. 2004. An application of AVHRR imagery used in combination with CORINE Land Cover data for forest-fire observations and consequences assessment. *International Journal of Applied Earth Observation and Geoinformation* 5(4): 263–274.

Simard, M., Saatchi, S. S., and G. De Grandi. 2000. The use of decision tree and multiscale texture for classification of JERS-1 SAR data over tropical forest. *IEEE Transactions on Geoscience and Remote Sensing* 38 (5): 2310–2321.

Steber, M., Allen, A., James, B., and K. Koss. 2012. Enhancing the capabilities of VLandgate's FireWatch with fire spread simulation. In *Proceedings of Bushfire CRC & AFAC 2012 Conference Research Forum Perth Australia*, R. Thornton, and L. Wright (eds.), Bushfire Cooperative Research Center, Australia, pp. 115–123.

Tappan, G., Tyler, D., Wehde, M., and D. Moore. 1992. Monitoring rangeland dynamics in Senegal with advanced very high resolution radiometer data. *Geocarto Internationala* 1: 87–98.

Umamaheshwaran, R., Bijker, W., and A. Stein. 2007. Image mining for modeling of forest fires from Meteosat images. *IEEE Transactions on Geoscience and Remote Sensing* 45: 246–253.

Ustin, S. L. 2004. *Manual of Remote Sensing*, vol. 4. Remote sensing for natural resource management and environmental monitoring, Wiley, NJ.

Vafeidis, A. T., and N. A. Drake. 2005. A two-step method for estimating the extent of burnt areas with the use of coarse-resolution data. *International Journal of Remote Sensing* 26(11): 2441–2459.

Van den Bergh, F., and P. Frost. 2005. A multi temporal approach to fire detection using MSG data. In *Proceedings of International Workshop on the Analysis of Multi-Temporal Remote Sensing Images*, Biloxi, MS, pp. 156–160.